ARTICLE

Achieving a Stable Time Response in Polymeric Radiation Sensors under Charge Injection by X-rays

Akarin Intaniwet,[†] Christopher A. Mills,[†] Paul J. Sellin,[†] Maxim Shkunov,[‡] and Joseph L. Keddie*[,†]

Department of Physics and Advanced Technology Institute, University of Surrey, Guildford, Surrey GU2 7XH, United Kingdom

ABSTRACT Existing inorganic materials for radiation sensors suffer from several drawbacks, including their inability to cover large curved areas, lack of tissue-equivalence, toxicity, and mechanical inflexibility. As an alternative to inorganics, poly(triarylamine) (PTAA) diodes have been evaluated for their suitability for detecting radiation via the direct creation of X-ray induced photocurrents. A single layer of PTAA is deposited on indium tin oxide (ITO) substrates, with top electrodes selected from Al, Au, Ni, and Pd. The choice of metal electrode has a pronounced effect on the performance of the device; there is a direct correlation between the diode rectification factor and the metal-PTAA barrier height. A diode with an Al contact shows the highest quality of rectifying junction, and it produces a high X-ray photocurrent (several nA) that is stable during continuous exposure to 50 kV Mo Kα X-radiation over long time scales, combined with a high signal-to-noise ratio with fast response times of less than 0.25 s. Diodes with a low band gap, 'Ohmic' contact, such as ITO/PTAA/Au, show a slow transient response. This result can be explained by the build-up of space charge at the metal-PTAA interface, caused by a high level of charge injection due to X-ray-induced carriers. These data provide new insights into the optimum selection of metals for Schottky contacts on organic materials, with wider applications in light sensors and photovoltaic devices.

KEYWORDS: sensor • conjugated polymer • organic electronics • charge transport • rectification • poly(triarylamine) (PTAA)

1. INTRODUCTION

A new generation of radiation sensors is required to improve on existing devices. Radiation detectors are needed for particle physics experiments (1), dosimetry in medical radiotherapy (2), and for security applications (3). Each of these applications has specific materials requirements that are driving further development.

Methods for the indirect detection of radiation rely on a secondary transduction method, such as the modulation or quenching of optical properties or scintillation in combination with a phosphor screen (4). In the latter type of indirect detector, the scintillation light is absorbed by a photoconductor or an optical sensor that generates a signal. Of more practical use, and the topic of the present work, is the direct detection of radiation. In this case, the radiation exposure induces a photocurrent in a semiconducting material that can be correlated with the radiation dose in a quantitative way. Direct detectors have higher sensitivity, lower signal noise, and improved spatial resolution compared to scintillation detectors. On the other hand, indirect detectors typically have a more complex and less efficient structure, particularly in medical dosimetry applications.

Solid-state radiation sensors for the direct detection of radiation have conventionally used either scintillation crystals or inorganic semiconductors, such as silicon, as charge-based detectors (5, 6). In detectors for synchrotron or linear accelerators used by particle physicists, large areas in curved geometries are needed. However, large-area, high-quality inorganic crystals are expensive and difficult to manufacture. The detector is limited to sizes up to eight inches for silicon, as defined by the requirements of the electronics industry, but limited to much smaller dimensions for other, more exotic crystalline materials.

In medical radiation dosimetry applications, on the other hand, there is a need for detectors that have tissue equivalence for dose estimations to the human body and that minimize beam perturbations (7). This requirement means that the detectors must be comprised of the elements of human tissue, e.g., C, H, and O. Inorganic semiconductors being applied in detectors, such as CdTe and ZnTe, are composed of heavy elements and hence are not tissue-equivalent. Detectors that are in regular contact with humans must be made from materials that are not toxic. Hence, Cd-containing materials are excluded from such applications. Furthermore, the high cost of single-crystal inorganic semiconductors is also driving the development of alternative material for detectors and sensors.

There are specific performance requirements for radiation sensors that must be met by any new material for direct radiation detection. The detector material should provide a low dark current (<1 nA), good rectification behavior, and a high charge-carrier mobility. Clearly, the requirements for sensor materials are demanding, yet conjugated polymers can potentially meet them.

* Corresponding author. E-mail: J.Keddie@surrey.ac.uk.
Received for review March 14, 2010 and accepted May 12, 2010
[†] Department of Physics, University of Surrey.
[‡] Advanced Technology Institute, University of Surrey.
DOI: 10.1021/am100220y

Published on Web 05/24/2010

Despite vibrant activity in the organic electronics field, the use of conjugated polymers for the detection of ionizing radiation has received comparatively little attention from the community. Conjugated polymers have, however, been used in indirect sensors of protons (8) and γ radiation (9), and polymer photodiodes have been used for scintillation detectors for X-rays (10−12). In comparison, semiconducting polymers are well-established for use as the active element in electronic devices, such as light emitting diodes (13), field effect transistors (14), photovoltaic cells (15) and chemical sensors (16). Polymers rival the performance of their inorganic semiconductor analogues, especially with respect to display and lighting technology (17).

The use of semiconducting polymers opens the possibility for large-area fabrication using low-cost, wet processing techniques, such as spin-casting, spray casting, inkjet or roll-to-roll printing (18). Polymers are flexible and so can be flexed to create curved detector surfaces. Their elemental composition makes them tissue equivalent and nontoxic. Their cost is comparable to some of the new inorganic semiconductor compositions.

Yoshino et al. established the possibility of using conjugated polymers for radiation sensing by studying the effects of electron irradiation on the conductivity of iodine-doped poly(acetylene) at room temperature (19). Recently, thick semiconducting polymer films have shown the potential of direct detection of alpha (α) particles (20, 21). We have recently shown that a direct X-ray induced photocurrent can be observed in metal/polymer/metal diode structures (22−24), thereby demonstrating the feasibility of using conjugated polymers in direct real-time radiation detection applications. However, the performance stability, measurement repeatability, and signal quality of such polymeric sensors upon exposure to X-rays, have not yet been determined. The question remains whether organic material-based sensors are suitable for solid-state radiation detection applications. More importantly, there is no clear design strategy in the materials selection for the development of high-performing sensors.

In this work, we have chosen a p-type poly(triarylamine) (PTAA) as the active material in metal/polymer/metal semiconductor diodes because of its long-term environmental stability (14, 25) and its relatively high charge-carrier mobility (1×10^{-2} cm^2/(V s)) (26). The fabrication and characterization of prototype organic semiconductor sensors using thick PTAA films, for use as charge-sensitive, direct-detection X-ray sensors, have already been presented (23, 24). Here, we have investigated the effects of the choice of metal for the top electrode by comparing the results obtained from Al, Au, Ni, and Pd. We thereby develop a general approach for the materials selection for metal contacts for organic-based sensors, which will form the basis for future device development for this application. The important parameters for device performance, including device stability, measurement repeatability, and signal-to-noise ratio, are assessed in the prototype sensors. Moreover, we have gained an improved understanding of the process of charge injection and stable time response in polymer diodes, which has relevance to other polymeric devices, including sensors and photovoltaics.

2. EXPERIMENTAL DETAILS

PTAA with weight-average molecular weight (M_w) of 31 kg/mol and a polydispersity (PDI) index (M_w/M_n) of 2.07 was synthesized by a method described elsewhere in the literature (27). Transparent ITO-coated glass, with a sheet resistance of 25 Ω and a deposited ITO thickness of 80−120 nm, was obtained from Delta Technology Ltd., USA (CB-60IN). Aluminum wire (analytical grade, 0.76 mm diameter, Fisher Scientific, UK), gold wire (0.2 mm diameter, Agar Scientific, U.K.), Ni target, and Pd target were used for electrode preparation. Toluene (99.99% purity) was used as received (Sigma Aldrich).

The details of the device preparation can be found elsewhere (23). In summary, a 5 wt % solution of PTAA in toluene was spin-cast on top of the ITO providing a single polymeric active layer thickness of either 20 or 30 μm. In the present work, the interfacial layer of poly(3,4 ethylene dioxythiophene): poly(styrene sulfonate) has been excluded from the diode structure, because it was found to have no effect on electrical properties in the devices. The PTAA films were initially left to dry under atmospheric conditions and then annealed under vacuum at 150 °C, which is above the glass transition temperature of the polymer ($T_g \approx 103$ °C) (23), for 12 h to eliminate any trapped solvent. The thickness profile of the active layer was subsequently measured using a surface profilometer (Dektak, Veeco Instruments). To complete the diodes, either gold (Au) and aluminum (Al) contacts (100 nm thick, 0.5 × 0.5 cm^2) were thermally evaporated onto the PTAA, at a pressure of 1×10^{-6} mbar, whereas either nickel (Ni) or palladium (Pd) were sputtered (JLS MPS 500 sputtering system) through a shadow mask to define an active area of the sensor. After attaching filament wires to the respective electrodes, the devices were encapsulated with plasticized bonding wax (Logitech Ltd., UK) by dip coating the diode in the molten wax. The X-ray attenuation efficiency of a 1 mm thick paraffin wax layer calculated by using values in a photon attenuation database (28) is approximately 5%. We neglect the effect of this wax layer when comparing the response of the devices to varying X-ray doses. The sensors were stored under nitrogen and in the dark to reduce any oxidation effects and to limit dust contamination.

The current−voltage ($I-V$) characteristics of the ITO/PTAA/metal diodes were examined using a voltage source-picoammeter (487, Keithley Instruments, U.K.) by applying a bias voltage from −100 to 100 V to the ITO electrode. Dosimetry measurements were performed using 17.5 keV Kα X-rays from a molybdenum target X-ray tube (XF50 11, Oxford instruments, U.K.). The anode current of the tube could be varied up to 1 mA at an operational anode voltage of 50 kV, providing X-ray dose rates up to 67 mGy/s. While applying a constant operating voltage to the ITO electrode, the sensor was exposed to the X-ray beam through the metal top electrode. The induced photocurrent was then measured using a voltage source-picoammeter (487, Keithley Instruments, U.K.). During exposure, the sensors were mounted in a steel box, in the dark and at room temperature, 10 cm from the X-ray source.

3. RESULTS AND DISCUSSION

The quality of the rectifying junction formed at the PTAA/metal interface was examined for various metal top contacts (Al, Au, Ni, or Pd) using a standard current−voltage measurement. Figure 1a shows the d.c. characteristics for each of the four diodes. Voltage was applied to the ITO electrode in all cases. The results show that the PTAA/Al interface forms an extremely good rectifying junction with a reverse

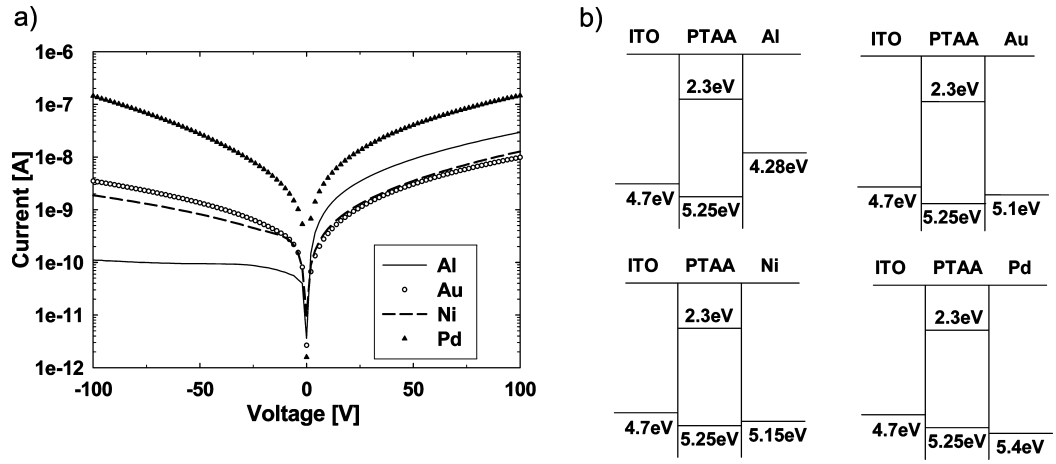

FIGURE 1. (a) Semilog current−voltage characteristic for the ITO/PTAA/metal diodes, with 20 μm thick PTAA layers, when using Al (—), Au (○), Ni (---), and Pd (▲) as the top metal contacts. (b) The corresponding band diagrams for the four ITO/PTAA/metal diodes.

leakage current density as low as 0.4 nA/cm^2 at −100 V and with a rectification factor, defined as the ratio between the forward and the reverse leakage currents, of 260. On the other hand, the PTAA/Au and PTAA/Ni interfaces form a semi-Ohmic contact with a higher leakage current (14 nA/cm^2 at −100 V for the ITO/PTAA/Au diode). The rectification factor diminishes to a value of 3 and 6, for the ITO/PTAA/Au and ITO/PTAA/Ni diodes, respectively. For the ITO/PTAA/Pd diode, the $I-V$ curve is symmetric, indicating an Ohmic behavior with an extremely high leakage current density of ca. 600 nA/cm^2 at −100 V.

The diode characteristics can be explained through consideration of the metal work functions in relation to the HOMO level of the PTAA. Figure 1b represents the corresponding band diagram for each of the ITO/PTAA/metal diode structures. The work functions for the metal top contacts, ϕ_m, are taken from ref 29. The HOMO value for PTAA is situated at approximately 5.25 eV according to cyclic voltammetry measurements (30−32), and the band gap energy, E_g, for PTAA was found to be 2.95 eV from previous PL spectroscopy (23). The barrier height for hole injection (ϕ_b) at the PTAA/metal interface can be evaluated using the following equation (16)

$$\phi_b = E_g - \phi_m + \chi_s \quad (1)$$

where χ_s is the electron affinity of the conjugated polymer. For PTAA, a value of 2.3 eV is used (see the band diagram). From eq 1, the PTAA/Al interface is found to have the highest barrier height for hole injection (Table 1) and hence provides a good quality Schottky junction with an exceptionally low reverse bias leakage current. For the PTAA/Au and the PTAA/Ni interfaces, the energy of the metal work function and the HOMO level of PTAA are relatively close to each other, and ϕ_b is calculated to be 0.15 eV. Therefore, the device displays an Ohmic behavior with a higher leakage current, rather than a Schottky behavior. The ITO/PTAA/Pd diode has the highest leakage current, due to the negative value of ϕ_b at the PTAA/Pd interface (−0.15 eV). This is an indication of an Ohmic contact in which the injected carriers (holes) can now flow in either direction without any resistance from the interface.

Table 1. Barrier Heights Calculated from the Band Diagrams in Figure 1b and the Corresponding $I-V$ Characteristics

interface	barrier height, ϕ_b (eV)	leakage current densities (nA/cm^2)	rectification ratio
PTAA/Al	0.97	0.4	260
PTAA/Au	0.15	14	3
PTAA/Ni	0.1	8	6
PTAA/Pd	−0.15	600	1

Time-dependent X-ray responses, after subtraction of the average dark current, for three different metal contacts (Au, Al, and Ni) are shown in Figure 2 for an applied voltage of 200 V. The ITO/PTAA/Pd diodes are unsuitable for X-ray detection because of their high dark current. It is not possible to detect the relatively low X-ray photocurrent generated within this device. Therefore, diodes with Pd contacts are not considered further here. The reverse bias in each device was achieved by applying a negative voltage at the ITO contact. The X-ray source, generating 17.5 keV X-rays from

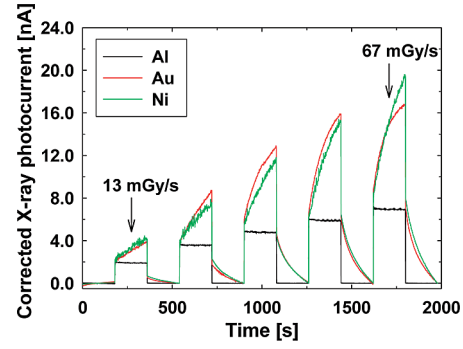

FIGURE 2. Time-dependent X-ray response for the ITO/PTAA/metal sensors, with 20 μm thick PTAA layers, at an operational voltage of 200 V, upon exposure of 17.5 keV X-rays for 180 s durations through Al (black line), Au (red line), and Ni (green line) top contacts with X-ray dose rates increasing over time (13, 27, 40, 54, and 67 mGy/s).

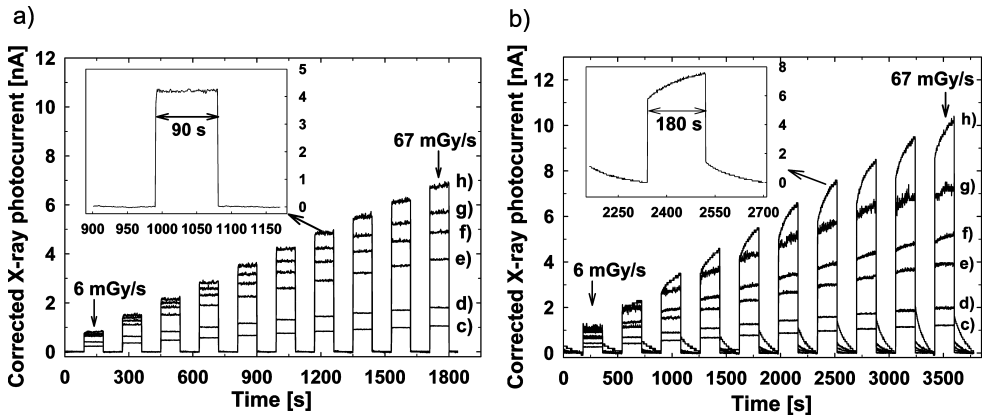

FIGURE 3. Response of the ITO/PTAA/metal sensors, with 30 μm thick PTAA layers, upon exposure to 17.5 keV X-rays through (a) Al and (b) Au top contacts with dose rates increasing over time (6, 13, 20, 27, 33, 40, 47, 54, 60, and 67 mGy/s). The devices are exposed to X-radiation for 90 s for the Al contact and for 180 s for the Au contact. Operational voltages: (c) 10, (d) 20, (e) 60, (f) 100, (g) 150, and (h) 300 V. Insets: magnified plot of a single response when exposed to an X-ray dose rate of 47 mGy/s and operated at 300 V.

a Mo target, is alternately turned on and off for periods of 180 s for each dose rate. With a reverse bias, the device produces a negative X-ray photocurrent; however, the data are presented here as a positive current. The response of the device with the highest quality of Schottky junction (i.e., the ITO/PTAA/Al diode) is fast when subjected to the X-ray beam. The X-ray photocurrent signal is stable over the period of exposure. On the other hand, the devices with a semi-Ohmic contact (the ITO/PTAA/Au and the ITO/PTAA/Ni diodes), display a fast response in the beginning, followed by a slow building in the X-ray photocurrent, which carries on over the time of exposure. For the ITO/PTAA/Au device at an operational voltage of 200 V and an X-ray dose rate of 67 mGy/s, a characteristic time constant of 71 s is obtained by fitting the slow component with an exponential function. When the X-rays are switched off, the signal drops sharply in the beginning and then shows a slow exponential decay component over time with a characteristic time constant of 79 s after irradiation. A higher time constant of 150 s was found for the ITO/PTAA/Ni device.

From our results, it is obvious that the X-ray response depends greatly on the type of the metal used as a top contact. That is, the quality of the Schottky junction formed at the PTAA/metal interface plays an essential role in the transient response. Therefore, the metal selection is very crucial for organic sensor fabrication. In general, the work function of the metal contact must be significantly lower than the HOMO energy level of a particular p-type organic semiconductor to achieve a suitable barrier height. In this particular case, a good Schottky junction is formed at the PTAA/Al interface, resulting in a stable photocurrent signal in the device.

Several authors have reported the observation of a slow transient response in organic photodiodes (33, 34), which is believed to be caused by the presence of electronic traps or defects in the organic semiconductor. The time constant for traps is typically in the range of a few ns for fast traps up to a few minutes for slow traps, depending on the energy level of traps in the material. In our study, we see a clear correlation between the transient performance of the measured X-ray induced photocurrent and the effective band gap of the Schottky junction at the metal/PTAA interface. The observed slow transient response of the ITO/PTAA/Au and the ITO/PTAA/Ni devices is in contrast to the fast response from the ITO/PTAA/Al device. Because all properties associated with the bulk material and the PTAA/ITO interfaces are identical between the diodes, it is clear that the nature of the metal/PTAA interface is responsible for the different transient behaviors.

Saito and Kobayashi observe similar transient phenomena in modulated photocurrent measurements of organic photocells (34), and they describe the observed slow time constants in terms of a modified space-charge distribution at the Schottky barrier. The optical injection of excess photocarriers causes the build-up of space-charge limited currents, which influence the effective Schottky barrier height because of band bending at the metal−polymer interface. In our data, these effects may be considerably enhanced because of the high density of X-ray generated free carriers throughout the PTAA layer. For the ITO/PTAA/Al system, with a larger effective band gap, the influence of X-ray induced space charge is minimized, and hence this device is more resistant to the formation of slow transients, even at high X-ray dose rates. By contrast, the low band gap devices—ITO/PTAA/Au and ITO/PTAA/Ni—are much more sensitive to small changes in the metal−PTAA interface because of space-charge build-up.

A transition in the X-ray response curve from a fast, stable response to a slow response is found when operating at a high voltage. Figure 3 demonstrates a typical dynamic X-ray photocurrent response, after subtraction of the average dark current, for 30 μm thick PTAA sensors with Al or Au electrodes, as a function of increasing bias voltage and increasing dose rate. The devices are operated under reverse bias conditions in which the ITO electrode is negatively biased. The dose rate of the incident X-rays is varied from 6 to 67 mGy/s, and the applied voltage is increased from 10 to 300 V. The X-ray photocurrent from the sensors increases as the dose rate of the incident X-rays increases and as the reverse bias applied to the diode increases.

Here, we have demonstrated the response of the sensor for only one X-ray energy (17.5 keV), but the sensors are

expected to show a similar trend of responses to X-rays of different energies. In general, the X-ray photocurrent from the PTAA-based sensor at a particular dose rate or applied voltage depends on the amount of X-rays being attenuated in the active material, which significantly varies with the X-ray energy and the thickness of the active layer (23). The X-ray attenuation coefficient can be calculated using the linear attenuation coefficient provided in a photon attenuation database (28) and used to determine the effect of the X-ray energy. For instance, the attenuation coefficient for a 30 μm thick PTAA layer upon 17.5 keV X-ray irradiation is 0.575 cm^2/g. The value reduces when subjected to a higher X-ray energy. The attenuation coefficient of the same PTAA layer is found to be 0.026 cm^2/g for an X-ray energy of 6 MeV, and therefore a lower X-ray photocurrent is expected at a higher X-ray energy.

Figure 3a shows the response of the ITO/PTAA/Al sensor as the X-ray tube is alternately switched on and off for 90 s for each dose rate. The response of the device when subjected to the X-ray beam (inset Figure 3a) is faster than the sampling rate of the measurement equipment (0.25 s). This holds true for all the applied operational voltages. The induced X-ray photocurrent at each X-ray dose rate is stable over the time of exposure, although the signal noise increases with applied voltage from 0.009 nA at 10 V (at a dose rate of 67 mGy/s) to 0.9 nA at 300 V.

The induced X-ray photocurrent for the ITO/PTAA/Au sensor is presented in Figure 3b. In this case, the X-ray source was alternately turned on and off for periods of 180 s. This device shows a stable X-ray photocurrent response at low dose rates (6 mGy/s) or low applied voltages (below 60 V). However, at either high dose rate or high voltage, the induced X-ray photocurrent signal can be divided into two components: an initially fast response followed by a slow increase in the current after approximately 0.5 s, which continues over the time of exposure (e.g., see inset of Figure 3b). Under these extreme conditions, the sensor is also slow to recover. After turning off the X-ray source, the current initially falls rapidly and then slowly decays to the dark current baseline over time. Similar behavior upon X-ray irradiation can also be seen for the ITO/PTAA/Ni sensor (not shown here) with a similar value of X-ray photocurrent as found with the ITO/PTAA/Au sensor.

Charge transport in the sensors can be described as follows. Excitons are usually created in the polymer layer after an X-ray photoexcitation process. An applied external electric field separates the excitons into free charge carriers (electrons and holes). Electron transport in conjugated polymers is extremely sensitive to impurities. Extrinsic effects, such as the presence of traps specifically for electrons, or the instability of radical anions upon the presence of water, oxygen and hydroxyl groups, are known to be responsible for the low mobility of electrons in conjugated polymers (35–37). Moreover, there is no observable electron transport in PTAA according to TOF results published elsewhere (25). Therefore, the X-ray response from our polymer sensors is mainly due to hole transport.

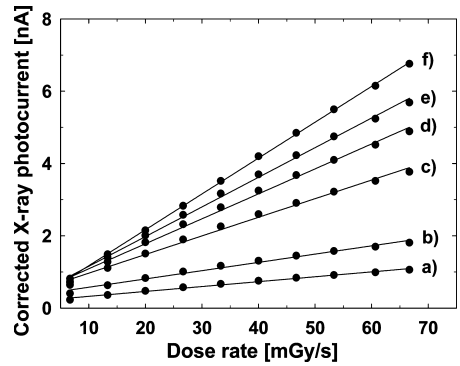

FIGURE 4. Corrected X-ray photocurrent as a function of X-ray dose rate for the ITO/PTAA/Al sensor with 30 μm thick PTAA active layers. Applied voltages are: (a) 10, (b) 20, (c) 60, (d) 100, (e) 150, and (f) 300 V. The error range on the data points is $\pm$0.07 nA, which is similar to the size of the symbols.

Table 2. Comparison of X-ray Sensitivity for the ITO/PTAA/Al and ITO/PTAA/Au Sensors

	sensitivity ($nC/mGy/cm^3$)	
voltage (V)	ITO/PTAA/Al	ITO/PTAA/Au
10	18	24
20	31	35
60	69	73
100	92	99
150	110	143
300	132	204

Figure 4 shows the corrected X-ray photocurrent as a function of the applied X-ray dose rate for the ITO/PTAA/Al device, which has been determined at several applied voltages using the data from Figure 3. The data show a linear relationship between the measured photocurrent and the X-ray dose rate, over a wide range of bias voltages from 10 to 300 V. The minimum operational voltage in our devices to yield sufficient sensitivity is approximately 10 V. This result can be compared with what is found in a Si p–n detector, which can be operated at an even lower bias, but normally is operated fully depleted at high voltage. The increase in photocurrent with bias voltage is consistent with the longer carrier drift length through the PTAA layer due to higher electric field strength. The linear response of the device as a function of increasing dose rate confirms that space charge build-up, and related charge injection phenomena, do not affect the device response in this dose rate regime.

To achieve sufficient sensitivity to radiation, it is essential that the signal from the induced photocurrent is greater than the background signal. In other words, the capability of the detection in the device is limited by the background signal (noise). Figure 4 demonstrates that if the dose rate of the X-ray falls below 5 mGy/s, the induced X-ray photocurrent from the PTAA-based sensors will be in a similar range to the dark current (less than 0.1 nA). This dose rate defines a detection limit for the sensors.

The performance of the devices has been determined in terms of the sensitivity to ionizing X-ray radiation (Table 2). The device sensitivity to X-rays was assessed by dividing the

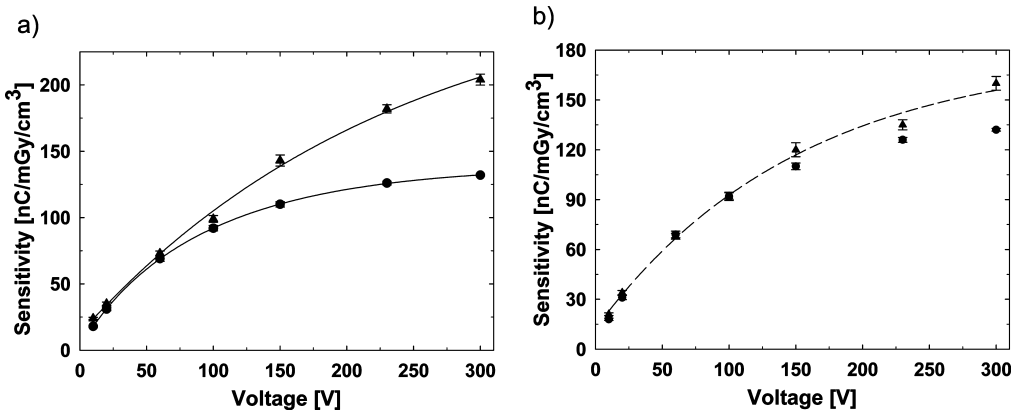

FIGURE 5. (a) Comparison of the sensitivity of the sensors, calculated using data from Figure 3, at different voltages, when using Al (•) or Au (▲) top contacts and 30 μm thick PTAA films. (b) Comparison of the sensitivity of the devices neglecting the slow component of the photocurrent from the ITO/PTAA/Au diode.

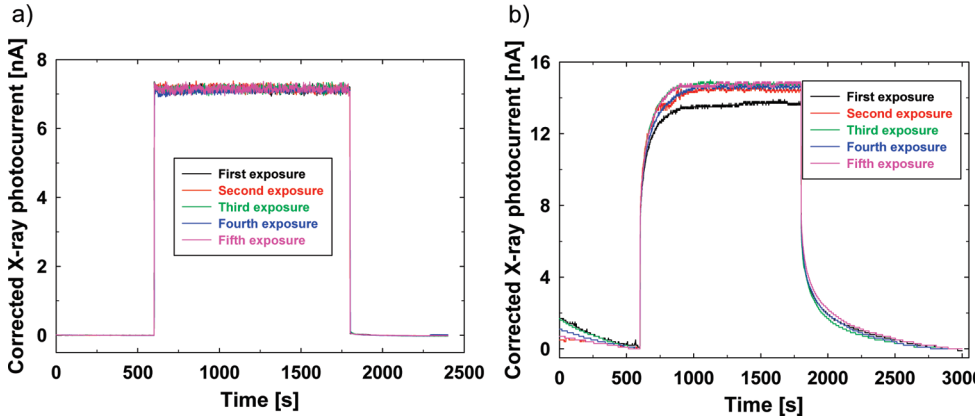

FIGURE 6. Corrected X-ray photocurrent response for (a) ITO/PTAA/Al and (b) ITO/PTAA/Au devices, with 30 μm thick PTAA layers, irradiated by X-rays at a dose rate of 67 mGy/s for 20 min and operated at 300 V. The plots show five repeat experiments performed on the same device.

slope of the X-ray photocurrent versus dose rate graph (Figure 4) by the active volume of the device. Figure 5a shows the increase in the detector sensitivity as the applied reverse bias increases. At low operational voltages (below 100 V), there is no difference in the device sensitivity using either Al or Au as the top electrode. At high applied voltages (above 100 V); however, the ITO/PTAA/Au device sensitivity is higher. The maximum sensitivity calculated for the ITO/PTAA/Al and the ITO/PTAA/Au sensors was 130 and 200 nC/mGy/cm^3, respectively. The sensitivity for both devices approaches a saturation value at high operational voltages. Similar results have been seen for a 20 μm thick PTAA sensor (not shown here). In calculating the sensitivity values presented in Figure 5a, the X-ray photocurrent obtained at the end of the exposure time was used. Both the fast and the slow components of the response of the ITO/PTAA/Au devices are considered.

For comparison, Figure 5b demonstrates the sensitivity of the devices to X-ray radiation when only the fast rising component of the X-ray photocurrent is considered: the slow component in the ITO/PTAA/Au sensor is ignored. In this case, the calculated sensitivity from both devices is very similar for each applied voltage and both asymptote toward a saturation value at a high reverse bias. The result indicates that the fast component of the response from both devices has the same origin, which derives from the carrier generation within PTAA molecules. The results clearly show that using an Au electrode provides an extra induced X-ray photocurrent in the sensor at high applied field, which may be used to produce a higher sensitivity to X-ray irradiation. However, the long current stabilization and device recovery times, arising from the slow component of the X-ray photocurrent signal, means that the device is less applicable for fast X-ray detection applications.

The performance of the PTAA sensors over a long period of exposure for five consecutive measurements is presented in Figure 6. Here, the most extreme case of exposure, an X-ray dose rate of 67 mGy/s and an operational voltage of 300 V, has been chosen to test the stability and repeatability of the signal from the devices. The sensors were exposed to the X-rays for 20 min, for a total dose of 80 Gy in each measurement. The response of the ITO/PTAA/Al device (Figure 6a) is again faster than the sampling rate of the measurement electronics (0.25 s). The induced X-ray photocurrent (7 nA) has a good stability over the time of measurement. The X-ray response for the ITO/PTAA/Au sensor (Figure 6b) is initially fast (<0.25 s) and then exhibits the slow exponential rise of the induced current to a saturation value of 15 nA with an average, characteristic time constant, τ = 77 s obtained by fitting to an exponential

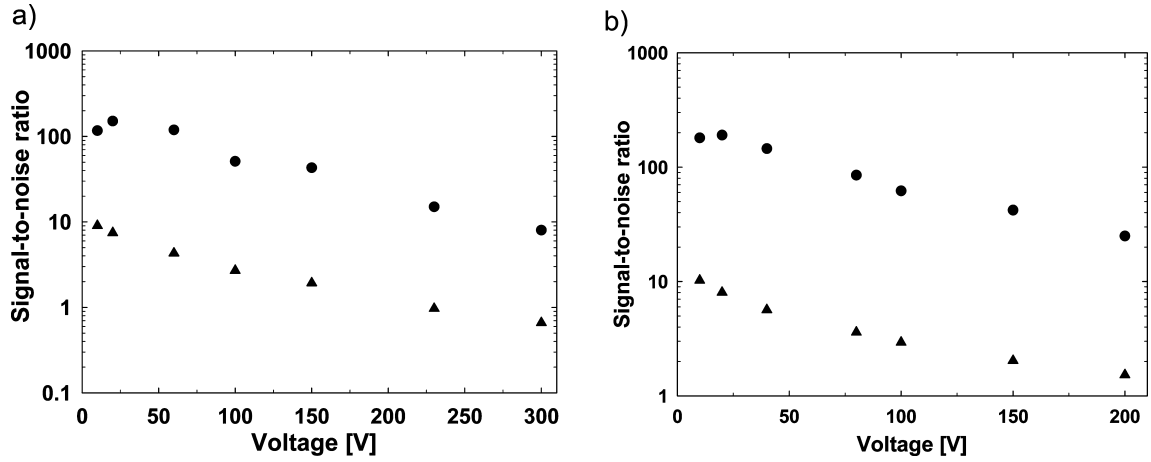

FIGURE 7. Signal-to-noise ratio as a function of the applied voltage obtained from (a) 30 and (b) 20 μm thick PTAA films, with Al (•) and Au (▲) top contacts. The data were taken when the devices are exposed to an X-ray dose rate of 67 mGy/s.

function. When the X-rays are turned off, the induced current initially falls quickly to a certain value and then has a slow exponential decay with an average, characteristic time constant of $\tau = 130$ s to the dark current baseline value. With the operational bias still applied, this slow decay of the charge is probably due to the detrapping of charge carriers. The results prove that our devices can be repeatedly operated under extreme conditions of radiation with no noticeable degradation of the polymer active layer for up to 100 min at 67 mGy/s.

Finally, the performance of the sensors has been evaluated in terms of the signal-to-noise ratio (Figure 7). The signal-to-noise ratio, defined as the corrected X-ray photocurrent divided by the dark current, was calculated using the data from Figure 3 at an X-ray dose rate of 67 mGy/s. Figure 7a shows that the signal-to-noise ratio for the ITO/PTAA/Al sensor is higher than that for the ITO/PTAA/Au sensor, with 30 μm thick PTAA layers in each case. This result indicates that the ITO/PTAA/Au device suffers from a higher dark current, which has been presented previously in current/voltage measurements. The semi-Ohmic Au/PTAA contact produces a high dark current when operated at a high reverse bias (ca. 10 nA at 300 V).

The Al/PTAA interface in the ITO/PTAA/Al sensor, on the other hand, produces a rectifying junction. The dark current, in this case, is extremely low when operated in reverse bias (see Figure 1A), which leads to a high signal-to-noise ratio. Figure 7b shows a similar result for the signal-to-noise ratio for sensors with a 20 μm thick PTAA layer. In detector applications, a low leakage current at high applied field is desirable in order to maximize the induced X-ray photocurrent. The use of the Al contact satisfies this requirement and produces a stable photocurrent even at high applied bias. It is noted that changing the contact area should not alter the signal-to-noise ratio because the dark current should scale with the contact area in the same way that the photocurrent will. But changing the bias voltage, the film properties, or the X-ray intensity will significantly alter the quality of the signal.

4. CONCLUSIONS

We have reported the successful fabrication of prototype organic sensors with 30 μm thick PTAA films as an active material for real-time direct X-ray detection. It has been shown that the PTAA devices can detect 17.5 keV X-ray radiation with dose rates as low as 6 mGy/s, and with sensitivities up to 200 nC/mGy/cm^3 for dose rates ranging up to 67 mGy/s.

It was discovered that the choice of electrode contact material has a large effect on device performance. A high rectification Schottky diode can be achieved using a metal with a work function lower than the HOMO level of the polymer. The resulting higher barrier height metal−polymer contact produces a fast time-independent response with very stable photocurrent output and a high signal-to-noise ratio. When using PTAA, it was found that Al is very suitable for the metal contact. The ITO/PTAA/Al devices show no discernible reduction in stability when exposed to a total of 400 Gy of X-rays over time periods up to 100 min. In contrast, diodes with lower barrier heights, fabricated with either Au or Ni contacts, show a long-lived, slow transient response to X-ray irradiation, because of X-ray-induced charge injection and the build-up of space charge close to the metal−polymer interface.

We conclude that when selecting the material for the contacts on a polymeric sensor, the metal's work function should lie between the HOMO and LUMO levels of the chosen polymer. Good induced current stability, high signal-to-noise ratio and measurement reproducibility demonstrate that PTAA can be used in real-time direct X-ray detection applications, provided that an Al (or similar) metal is used as the contact. These results are more widely applicable to polymer diodes operating in a high charge-injection regime, such as in photovoltaic devices or light sensors.

Acknowledgment. A.I. acknowledges a scholarship from the Office of the Higher Education Commission of the Royal Thai Government. The authors acknowledge financial support from the Science and Technology Facilities Council (STFC) (Grant ST/F006667/1). Dr. Heiko Thiem (Evonik Degussa GmbH, Germany) kindly supplied the PTAA. The

authors thank Dr. Veeramani Perumal, Gary Strudwick, Violeta Dukova (Department of Physics, University of Surrey), and Dean Mansfield (Advanced Technology Institute, University of Surrey) for help with diode preparation and characterization.

REFERENCES AND NOTES

(1) Moser, H.-G. *Prog. Part. Nucl. Phys.* **2009**, *63*, 186.
(2) Nava, F.; Bertuccio, G.; Cavallini, A.; Vittone, E. *Meas. Sci. Technol.* **2008**, *19*, 102001.
(3) Harding, G.; Schreiber, B. *Radiat. Phys. Chem.* **1999**, *56*, 229.
(4) Newman, C. R.; Sirringhaus, H.; Blakesley, J. C.; Speller, R. *Appl. Phys. Lett.* **2007**, *91*, 142105.
(5) Bos, A. J. J. *Nucl. Instrum. Methods Phys. Res., Sect. B* **2001**, *184*, 3.
(6) Milbrath, B. D.; Peurrung, A. J.; Bliss, M.; Weber, W. J. *J. Mater. Res.* **2008**, *23*, 2561.
(7) Yaparpalvi, R.; Fontenla, D. P.; Vikram, B. *Int. J. Radiat. Oncol. Biol. Phys.* **2000**, *48*, 1259.
(8) Lee, K. W.; Mo, K. H.; Jang, J. W.; Lee, C. E. *J. Kor. Phys. Soc.* **2005**, *47*, 130.
(9) Silva, E. A. B.; Borin, J. F.; Graeff, C. F. O.; Netto, T. G.; Bianchi, R. F. *Appl. Phys. Lett.* **2005**, *86*, 131902.
(10) Blakesley, J. C.; Keivanidis, P. E.; Campoy-Quiles, M.; Newmann, C. R.; Jin, Y.; Speller, R.; Sirringhaus, H.; Greenham, N. C.; Nelson, J.; Stavrinou, P. *Nucl. Instrum. Methods Phys. Res., Sect. A* **2007**, *580*, 774.
(11) Agostinelli, T.; Campoy-Quiles, M.; Blakesley, J. C.; Speller, R.; Bradley, D. D. C.; Nelson, J. *Appl. Phys. Lett.* **2008**, *93*, 203305.
(12) Kingsley, J. W.; Pearson, A. J.; Harris, L.; Weston, S. J.; Lidzey, D. G. *Org. Electron.* **2009**, *10*, 1170.
(13) Rathnayake, H. P.; Cirpan, A.; Delen, Z.; Lahti, P. M.; Karasz, F. E. *Adv. Funct. Mater.* **2007**, *17*, 115.
(14) Sirringhaus, H. *Adv. Mater.* **2005**, *17*, 2411.
(15) Tang, W.; Chellappan, V.; Liu, M.; Chen, Z.-K.; Ke, L. *ACS Appl. Mater. Interfaces.* **2009**, *1* (7), 1467.
(16) Potje-Kamloth, K. *Chem. Rev.* **2008**, *108*, 367.
(17) Choi, M.-C.; Kim, Y.; Ha, C.-S. *Prog. Polym. Sci.* **2008**, *33*, 581.
(18) Krebs, F. C. *Sol. Energy Mater. Sol. Cell.* **2009**, *93*, 394.
(19) Yoshino, K.; Hayashi, S.; Inuishi, Y. *Jpn. J. Appl. Phys.* **1982**, *21*, 569.
(20) Beckerle, P.; Ströbele, H. *Nucl. Instrum. Methods Phys. Res., Sect. A* **2000**, *449*, 302.
(21) Natali, D.; Sampietro, M. *Nucl. Instrum. Methods Phys. Res., Sect. A* **2003**, *512*, 419.
(22) Boroumand, F. A.; Zhu, M.; Dalton, A. B.; Keddie, J. L.; Sellin, P. J.; Gutierrez, J. J. *Appl. Phys. Lett.* **2007**, *91*, 033509.
(23) Intaniwet, A.; Mills, C. A.; Shkunov, M.; Thiem, H.; Keddie, J. L.; Sellin, P. J. *J. Appl. Phys.* **2009**, *106*, 064513.
(24) Mills, C. A.; Intaniwet, A.; Shkunov, M.; Keddie, J. L.; Sellin, P. J. *Proc. SPIE* **2009**, *7449*, 74491.
(25) Barard, S.; Heeney, M.; Chen, L.; Cölle, M.; Shkunov, M.; McCulloch, I.; Stingelin, N.; Philips, M.; Kreouzis, T. *J. Appl. Phys.* **2009**, *105*, 013701.
(26) Zielke, D.; Hübler, A. C.; Hahn, U.; Brandt, N.; Bartzsch, M.; Fügmann, U.; Fischer, T.; Veres, J.; Ogier, S. *Appl. Phys. Lett.* **2005**, *87*, 123508.
(27) Yamamoto, T.; Ito, T.; Kubota, K. *Chem. Lett.* **1988**, *17*, 153.
(28) Berger, M. J.; Hubbell, J. H.; Seltzer, S. M.; Chang, J.; Coursey, J. S.; Sukumar, R.; Zucker, D. S. *XCOM: Photon Cross Sections Database*; National Institute of Standards and Technology: Gaithersburg, MD; http://physics.nist.gov/PhysRefData/Xcom/Text/XCOM.html; also called Standard Reference Database 8 (XGAM).
(29) Kaye, G. W. C., Laby, T. H. *Table of Physical and Chemical Constants*, 16th ed.; Longman Group Limited: London, 1995.
(30) Kisselev, R.; Thelakkat, M. *Macromolecules.* **2004**, *37*, 8951.
(31) Thelakkat, M. *Macromol. Mater. Eng.* **2002**, *287*, 442.
(32) Choi, K.; Kwak, J.; Lee, C.; Kim, H.; Char, K.; Kim, D. Y.; Zenteh, R. *Polym. Bull.* **2008**, *59*, 795.
(33) Sharma, G. D.; Saxena, D.; Roy, M. S. *Synth. Met.* **1999**, *107*, 197.
(34) Saito, K.; Kobayashi, S. *Jpn. J. Appl. Phys.* **2003**, *42*, L781.
(35) Kazukauskas, V.; Tzeng, H.; Chen, S. A. *Appl. Phys. Lett.* **2002**, *80*, 2017.
(36) Smits, E. C. P.; Anthopoulos, T. D.; Setayesh, S.; van Veenendaal, E.; Coehoorn, R.; Blom, P. W. M.; de Boer, B.; de Leeuw, D. M. *Phys. Rev. B* **2006**, *73*, 205316.
(37) Chua, L. L.; Zaumseil, J.; Chang, J. F.; Ou, E. C. W.; Ho, P. K. H.; Sirringhaus, H.; Friend, R. H. *Nature* **2005**, *434*, 194.

AM100220Y